Enhanced Carbon, Nitrogen and Phosphorus removal from domestic wastewater in a novel anoxic-aerobic photobioreactor coupled with biogas upgrading.

Dimas García[1], Cynthia Alcántara[1], Saúl Blanco[2], Rebeca Pérez[1], Silvia Bolado[1], Raúl Muñoz[1]*

1- Department of Chemical Engineering and Environmental Technology, Valladolid University, Dr. Mergelina, s/n, 47011, Valladolid, Spain

2- The Institute of the Environment, La Serna 58 - 24007 León, Spain

* Corresponding author: mutora@iq.uva.es

1. Introduction

The steady increase in human population [1] and industrial activity is generating large amounts of wastewaters and greenhouse gases [2], which represent two of the major environmental challenges to global sustainability nowadays. Domestic and industrial wastewaters and anaerobic digestion effluents are characterized by their high loads of carbon (C), nitrogen (N) and phosphorus (P), which must be treated before discharge into natural water bodies to avoid oxygen depletion, toxicity issues and eutrophication [3]. A wide range of biological and physical/chemical technologies is currently available for carbon and nutrient removal in wastewater treatment plants (WWTPs). Unfortunately, these technologies often entail high investment and operating costs and do not allow for a cost-effective recovery of nutrients due to the low C/N and C/P ratios of most domestic and industrial wastewaters [4][5].

In this context, algal-bacterial processes can support both a low-cost process oxygenation and an enhanced nutrient recovery. The oxygen produced by microalgae during photosynthesis can support the oxidation of organic pollutants and ammonium by aerobic heterotrophs and nitrifiers, respectively, which thus reduces the operating costs and environmental impacts associated with conventional mechanical aeration in WWTPs [6]. On the other hand, the ability of algal-bacterial consortia to assimilate both organic carbon (inherently present in most wastewaters) and inorganic carbon (from the biological oxidation of organic carbon, alkalinity in wastewater or residual carbon dioxide (CO_2) externally supplied) result in larger biomass productivities and therefore enhanced nutrient recoveries[7]. However, despite the above-mentioned advantages, algal-bacterial processes devoted to wastewater treatment still present severe technical

limitations that hinder the full-scale implementation of this technology, such as nutrient supply and recycling, gas transfer and exchange [8].

In this regard, although photoautotrophic algal metabolism can enhance N and P recovery in anoxic-aerobic algal-bacterial photobioreactor (AA-ABPh), the alkalinity present in raw wastewaters is low to support a complete nutrient recovery/removal and residual CO_2 sources (such as flue gas) are not always available on-site. In addition, the low hydraulic retention times (HRT) required in algal-bacterial processes to compete with activated sludge systems would limit the development of nitrifying bacterial communities that would eventually support nitrification-denitrification processes during the treatment of wastewaters with low C/N ratios. Finally, the poor sedimentation ability of the microalgae generated in the process often results in effluent total suspended solid concentrations (TSS) above the maximum European Union (EU) discharge limit (50 mg/L), which limits the scale-up of microalgae-based wastewater treatment [9]. In this context, AA-ABPh operated with autofloculated biomass settling and recycling constitutes an innovative technology capable of overcoming the above mentioned limitations. This technology was successfully evaluated for the treatment of synthetic wastewaters at moderate HRTs but experienced severe inorganic carbon limitations, which ultimately restricted the treatment potential of this innovative technique. Therefore, there is an urgent need to develop novel operating strategies to overcome the above mentioned inorganic carbon limitation and to evaluate the performance of this innovative technology using real domestic wastewater (RDWW) at low HRTs.

This work was devised to evaluate the treatment of RDWW in an innovative AA-ABPh configuration operated with biomass settling and recycling at a HRT of 2 days coupled to the simultaneous upgrading of synthetic biogas (in a separate and interconnected column). In this system, the supply of biogas (eventually available on-site from the anaerobic digestion of the algal-bacterial biomass produced in the process) will provide the additional inorganic C source required to boost nutrient removal by assimilation and bacterial nitrification to sustain an efficient nitrification-denitrification process [10][11]. The influence of photosynthetic biogas upgrading on the mechanisms underlying C, N and P removal in the anoxic tank and photobioreactor treating RDWW was assessed using a mass balance approach. A detailed characterization of the dynamics of microalgal and bacterial population structure was conducted using morphological and molecular identification tools.

2. Materials and methods

2.1. Microorganisms and culture conditions

The anoxic and aerobic tanks were inoculated with 3.2 g/L of total suspended solid (TSS) of an mixture of a microalgal-cyanobacterial consortium (from now on referred to as microalgae) from a high rate algal ponds (HRAP) treating diluted vinasse [12] and aerobic activated sludge from Valladolid WWTP (Spain). Domestic wastewater was collected from a nearby sewer located at Department of Chemical Engineering and Environmental Technology of Valladolid University. The average composition of the RDWW treated continuously was: 176±26 mg/L of dissolved total organic carbon (TOC), 152±34 mg/L of dissolved inorganic carbon (IC), 106±9 mg/L of total nitrogen

(TN), 93±9 mg/L of N-ammonium ($N\text{-}NH_4^+$), 39±12mg/L of sulfate (SO_4^{2-}) and 33±8 mg/L of P-phosphate ($P\text{-}PO_4^{3-}$) (Table 1).

2.2. Experimental set-up

Three operational stages (SI, SII and SIII) were carried out in the experimental set-up below described to evaluate the influence of biogas supply and internal recycling rate on WWT performance. The experimental set-up during stage I (SI) consisted of an anoxic tank, with a total working volume of 0.9 L, interconnected to a photobioreactor with a total working volume of 2.7 L. Both reactors were operated as completely mixed flow reactors. The anoxic tank was maintained in the dark and magnetically stirred at 320 rpm. The photobioreactor was continuously illuminated for 12 hours/day (05:00h to 17:00h) by LED lamps arranged in a concentric configuration providing an average light intensity of 392±19 μmol/m^2·s at the outer wall of the photobioreactor (Figure 1). Air was introduced during the dark period in order to maintain the dissolved O_2 concentration in the photobioreactor above non-limiting concentrations [13][14] (Table 1). The temperature and magnetic agitation of the photobioreactor were maintained constant at 25±1°C and 320 rpm, respectively. During stage II (SII) and stage III (SIII), the photobioreactor was interconnected to a 0.3 L external absorption column (Ø = 2.54 cm; height = 60 cm) in order to provide an extra source of CO_2 via photosynthetic biogas upgrading (Figure 1).

< Figure 1>

2.3. Experimental design

The HRT and the Sludge Retention Time (SRT) were maintained at 2 days (HRT_{anoxic} = 0.5 day, $HRT_{aerobic}$ = 1.5 days) and ≈ 11 days, respectively, during the whole experiment (Table 1). These short HRTs are required to make algal-bacterial processes competitive with activated sludge systems. The experimental design was based on the operational limitations identified in previous studies in this AA-ABPh configuration [13][14]. The experiment was divided in three operational stages. The internal recycling (IR) flow rate from the photobioreactor to the anoxic tank was maintained at 2.8 L/d during SI (maintained for 78 days) and SII (maintained for 74 days), while this parameter was increased by 30% (3.6 L/d) during SIII (maintained for 56 days) in order to evaluate the maximum denitrifying capacity in the anoxic tank to ultimately boost the dissimilatory N removal in the experimental system. The external recycling flow rate (ER) from the settler to the anoxic tank was maintained at 0.5 L/d during the three operational stages (Table 1). The pH in the photobioreactor was maintained between 7.0 and 8.6 during SI by daily addition of 1.2 mL of chlorhydric acid (37%), while biogas upgrading into the absorption column supplied CO_2 to overcome the IC limitation encountered during SI and to maintain the pH below inhibitory values for bacterial activity (< 9) during SII and SIII. The synthetic biogas mixture supplied was composed of methane (70%), carbon dioxide (29.5%) and hydrogen sulfide (0.5%) (Abello Linde, Barcelona, Spain). Biogas was supplied to the absorption column at 2.6 L/d (1.8 ml/min) through a 10 µm metallic sparger located at the bottom of the column co-currently with a recycling algal-bacterial broth stream drawn from the photobioreactor at a liquid to biogas ratio (L/G) of 10 (v/v) (Figure 1). Liquid samples of 100 ml were taken twice per week from the RDWW, anoxic tank, aerobic tank, settled biomass and effluent to determine concentrations of TOC, IC, TN, $N\text{-}NH_4^+$, $N\text{-}NO_2^-$, $N\text{-}NO_3^-$, SO_4^{2-}, $P\text{-}PO_4^{3-}$ and TSS. pH, temperature and dissolved oxygen concentration (DO) were measured daily in both

bioreactors. Likewise, the C, N and P content of the algal bacterial biomass was measured under steady state at each operational stage. The sludge volumetric index (SVI) and the maximum biomass settling rate, which were used to monitor the settling characteristics of the algal-bacterial biomass [15], were determined in the anoxic and aerobic bioreactors under steady state at each operational stage. The microalgae population structure was assessed at the end of SI, SII and SIII using biomass samples from the photobioreactor preserved with lugol acid at 5% and formaldehyde at 10%, and stored at 4 ºC prior to analysis. Biomass samples from the photobioreactor were collected at the end of each steady state, and immediately stored at -20 ºC in order to evaluate the richness and composition of the bacterial communities [14]. Finally, the composition of the biogas at the inlet and outlet of the absorption column was determined twice a week during SII and SIII.

<Table 1>

2.4. Mass balance

The dilution effect in the anoxic tank caused by the internal and external recirculations was considered by calculating a virtual concentration for each parameter in the influent wastewater to the anoxic tank. Hence, the actual C, N and P removals in the denitrification reactor were assessed using the virtual concentrations (V*i*) for dissolved IC, TOC, N-NH_4^+ and P-PO_4^{3-} at the entrance of the anoxic tank according to Eq. (1):

$$V_i\left(\frac{mg}{L}\right) = \frac{(C_{i\,feed}\cdot Q_{feed})+(C_{i\,aerobic}\cdot Q_{RI})+(C_{i\,aerobic}\cdot Q_{RE})}{Q_{feed}+Q_{RI}+Q_{RE}} \quad (1)$$

where $C_{i\ feed}$ and $C_{i\ aerobic}$ represent the dissolved concentrations of the parameter "*i*"= TOC, IC, TN, N-NH_4^+ and P-PO_4^{3-} in the RWW and the photobioreactor, respectively,

while Q_{feed} represents the RDWW flow rate, Q_{RI} the internal recirculation flow rate and Q_{RE} the external recirculation flow rate.

An overall mass balance to the anoxic-aerobic photobioreactor was conducted for TOC, IC, TN, N-NH_4^+ and P-PO_4^{3-} based on their average concentrations under steady state conditions for each operational stage. The validity of the instrumental and analytical methods was thus assessed by means of the mass recovery factors for the parameter "*i*" according to Eq. (2) [14]:

$$M_i\ Recovery\ (\%) = \frac{(M_{i\,rem})\boldsymbol{anox} + (M_{i\,rem})\boldsymbol{photobior} + (M_i)\boldsymbol{effl}}{(M_i)RWW} \cdot 100 \qquad (2)$$

where $(M_{i\,rem})_{anoxic}$ and $(M_{i\,rem})_{photobior}$ represent the mass flow rate (g/d) of the parameter ***i*** = TOC, IC, TN, N-NH_4^+ and P-PO_4^{-3} removed in the anoxic tank and photobioreactor, respectively. $M_{i\,effl}$ and $M_{i\,RWW}$ represent the mass flow rate (g/d) of the parameter in the treated effluent and RWW, respectively.

The removal efficiencies herein reported for each tank refer to the individual contribution of the anoxic and photobioreactor units to the overall removal of the inlet loading for each monitored parameter.

2.5. Analytical procedures

The light intensity was measured as photosynthetically active radiation (PAR) using a LI-250A light meter (LI-COR Biosciences, Germany). Biogas composition was determined using a Bruker 430 GC-TCD (Palo Alto, USA) equipped with a CP-Molsieve 5A (15 m × 0.53 mm × 15 µm) and a CP-Pora BOND Q (25 m × 0.53 mm ×

15 µm) columns. The injector, detector and oven temperatures were maintained at 150 ºC, 175 ºC and 40 ºC, respectively. Helium was used as the carrier gas at 13.7 cm^3/min[16]. TOC, IC and TN concentrations were measured using a TOC-V CSH analyzer equipped with a TNM-1 module (Shimadzu, Japan). $N\text{-}NH_4^+$ was measured using the Nessler analytical method [15] in a U-2000 spectrophotometer (Hitachi, Japan), while NO_2^- and NO_3^- were determined by the cadmium reduction column method [15]. $P\text{-}PO_4^{-3}$ and SO_4^{2-} were analyzed by high performance liquid chromatography-ion chromatography (HPLC-IC) with a Waters 515 HPLC pump coupled with a Waters 432 ionic conductivity detector and equipped with an IC-Pak Anion HC (150 mm × 4.6 mm) waters column. A 510 pH meter (EUTECH Instrument, The Netherlands) was used for pH determination. DO concentration and temperature were recorded using an OXI 330*i* oximeter (WTW, Germany). The determination of the TSS concentration, SVI and settling rate were conducted according to Standard Methods [15]. The analysis of the C and N biomass content was carried out using a LECO CHNS-932 elemental analyzer with pre-dried and grinded algal-bacterial biomass. The content of P in the biomass was measured using a 725-ICP Optical Emission Spectrophotometer (Agilent, USA) at 213.62 nm. The identification, quantification and biometry measurements of microalgae were conducted by microscopic examination (OLYMPUS IX70, USA) of the algal-bacterial cultivation broths according to Phytoplankton Manual [17].

Genomic DNA was extracted using the protocol described in the Fast® DNA Spin Kit for Soil (MP Biomedicals, LLC) handbook. The V6-V8 regions of the bacterial 16S ribosomal ribonucleic acid (rRNA) genes were amplified by Polymerase Chain Reaction (PCR) analysis using the universal bacterial primers 968-F-GC and 1401-R

(Sigma-Aldrich, St. Louis, MO, USA; [18]). The PCR mixture contained 1 μL of each primer (10 ng μL-1 each primer), 25 μL of BIOMIX ready-to-use 2 reaction mix (Bioline, Ecogen), 2 μL of the extracted DNA and Milli-Q water up to a final volume of 50 μL. The PCR thermo-cycling program consisted of 2 min of pre-denaturation at 95°C, 35 cycles of denaturation at 95°C for 30 s, annealing at 56°C for 45 s, and elongation at 72°C for 1 min, with a final 5-min elongation at 72°C. The denaturing gradient gel electrophoresis (DGGE) analysis of the amplicons was performed with a D-Code universal mutation system (Bio Rad Laboratories) using 8% (w/v) polyacrylamide gels with a urea/formamide denaturing gradient of 45 to 65%. DGGE running conditions were applied according to Roest et al. (2005) [19]. The gels were stained with GelRed Nucleic Acid Gel Stain (biotium) for 1 h. The most relevant bands were excised from the DGGE gel in order to identify the bacteria present in the samples, resuspended in 50 μL of ultrapure water and maintained at 60 °C for 1hour to allow DNA extraction from the gel. A volume of 5 μL of the supernatant was used for reamplification with the original primer set. Before sequencing, PCR products were purified with the GenElute PCR DNA Purification Kit (Sigma-Aldrich, St. Louis, MO, USA). DGGE profiles were compared using the GelCompar IITM software (Applied Maths BVBA, Sint-Martens-Latem, Belgium). After image normalization, bands were defined for each sample using the bands search algorithm within the program. The peak heights in the densitometric curves were also used to determine the Shannon-Wiener diversity index (H). Therefore, this index reflects both the sample richness (relative number of DGGE bands) and evenness (relative intensity of every band). It ranges from 1.5 to 3.5 (low and high species evenness and richness, respectively) and can be calculated according to Eq. (3)[20]:

$$H = -\sum \left[P_i \ln(P_i) \right] \quad (3)$$

Where H is diversity index and P_i is the importance probability of the bands in a lane ($P_i = n_i/n$, where n_i is the height of an individual peak and n is the sum of all peak heights in the densitometric curves). Similarity indices of the compared profiles were calculated from the densitometric curves of the scanned DGGE profiles by using the Pearson product–moment correlation coefficient [21].The taxonomic position of the sequenced DGGE bands was obtained using the RDP classifier tool (50% confidence level) [22]. The closest cultured and uncultured relatives to each band were obtained using the BLAST search tool at the NCBI (National Centre for Biotechnology Information) [23]. The sequences generated from this work are deposited in GenBank under accession numbers KU854389-KU854421.

2.6. *Statistical analysis*

The data displayed in Table 1, Figure 2 and Figure 7(c) correspond to the mean ± standard deviation of the target parameters during steady state at each operational stage. A one-way ANOVA analysis was performed to assess any significant difference between the settling rate of the biomass from the anoxic reactor and the photobioreactor using Excel (Microsoft, USA). A Pearson correlation analysis was conducted to determine the similarity indexes among the population established during steady state operation.

3. Results and Discussion

The mass balance calculations over the 208 days of operation showed recoveries for TOC, IC, TN and $P\text{-}PO_4^{3-}$ of 100±1%, 99±4%, 100±5% and 100±14%, which validated

the analytical and instrumental methodologies used in this study. This mass balance approach allowed to better understand the symbiosis between microalgae and bacteria in this novel anoxic-aerobic algal-bacterial photobioreactor configuration [14], by quantifying the extent of the mechanisms involved in C, N and P removal in each reactor.

The overall removal efficiency of organic matter measured as TOC under steady state operation averaged 89±2% along the 3 operational stages at 2 days of HRT due to the high photosynthetic oxygenation capacity and denitrification activity of the system. In this context, while the DO concentration in the anoxic tank remained close to 0 mg O_2/L (thus supporting an efficient denitrification since the O_2 carried out by the internal recycling was lower that O_2 demand of the RDWW), the DO in the photobioreactor fluctuated from 15 and 32 mg O_2/L during illuminated periods to 1.5 and 7 mg O_2/L during dark periods in the photobioreactor (supplementary material Figure S1). These oxygen concentrations were sufficient to satisfy the bacterial demand from NH_4^+ and TOC oxidation in the photobioreactor. The organic matter removal recorded in this study was similar to that typically achieved in conventional activated sludge systems (COD-REs of 85-90%) and in conventional HRAPs treating domestic wastewater (COD-REs 81-88%). The high light intensity used in this lab-scale study to boost microalgae photosynthetic activity (392±19 μmol/m^2·s) supported an efficient overall steady state IC removal (95±4%) mainly based on microalgae assimilation, nitrification representing a minor IC removal mechanism (≈4.1% of the total IC input).

On the other hand, the average TN removal during SI under steady state operation accounted for 38±6% with average NH_4^+ removals of 39±9%. This low TN-RE was due to the low efficiency of NH_4^+ nitrification during SI as a result of a severe IC limitation.

Biogas supplementation in SII and SIII overcame this limitation and promoted steady state removals of TN and NH_4^+ of 81±3%, 97±2%, respectively, at a HRT of 2 days. NH_4^+ nitrification in the photobioreactor was the key step to ensure an efficient nitrogen removal in the anoxic tank via denitrification, despite NH_4^+ oxidation during SI was limited by the active photosynthetic IC uptake by microalgae. Comparable TN-REs ranging from 68% to 85% and N-NH_4^+-REs of 80-93% are typically achieved in CO_2-supplemented HRAPs treating domestic wastewater but at HRTs of 3-7 days, with nitrogen assimilation into biomass and NH_3 stripping identified as the main nitrogen removal mechanisms [24]. Lower TN-REs ranging from 57% to 73% are often achieved in HRAPs during the treatment of domestic sewage without CO_2 supplementation at HRTs of 3-10 days, which highlights the superior performance of our two-stage photobioreactor [25]. In addition, the values hereby obtained for nitrogen removal were comparable with the removal efficiencies of ≈ 80% typically reported in nitrification-denitrification activated sludge plants, although conventional WWTPs operate at 0.5-1 day of HRT [26].

Finally, average orthophosphate removal efficiencies of 59±17% were recorded under steady state operation in SI. However, the supplementation of biogas resulted in an enhanced biomass growth and therefore in a slight increase in P-PO_4^3-REs up to steady state values of 67±13% and 60±6% in SII and SIII, respectively. Bioassimilation into algal-bacterial biomass was likely the main phosphorous removal mechanism since pH values fluctuated from 6.8 to 9.4 during illuminated periods and from 6.4 to 8.1 during the dark periods in the photobioreactor (supplementary material Figure S1). The average pH values recorded along the entire experiment were likely not sufficient to support phosphate precipitation, which has been shown to occur at pHs > 9.0 [6][27]. The P-

PO_4^{3-}-REs here obtained (59 - 67%) were similarly those typically reported in HRAPs (50% to 75%) at significantly higher HRTs (3 – 7 days) and activated sludge processes at HRTs of 0.5 - 1 days [24]. However, the volumetric PO_4^{3-} removal rates achieved were superior based on the fact that the phosphate concentration in the RWW used in this study (33±8 mg P/L) was ≈ 5 times higher than the P-PO_4^{3-} concentrations typically present in medium strength WW (≈ 7 mg P/L)[28] (Table 1).

Finally, the high robustness of this process configuration should be highlighted based on the consistent effluent concentrations of TOC, IC, NH_4^+, TN, PO_4^{3-} despite the inherent variations of these parameters in RDWW.

3.1. Carbon and nutrient removal in the anoxic reactor

The overall removal efficiencies of TOC in the anoxic reactor accounted for 77±4% under steady state operation, with values of 77±4%, 76±6% and 79±3% for SI, SII and SIII, respectively (Figure 2a). This heterotrophic TOC removal (organic matter acting as electron donor) resulted in steady state concentrations of 27±5 mg/L in the anoxic tank regardless of the operational stage [29]. On other hand, a negative IC removal efficiency of -14±13% was recorded during SI as a result of CO_2 production from TOC oxidation in the anoxic tank (mainly driven by the use of O_2 as electron acceptor, which represented 67% of the total e^- acceptor consumption during SI) and the absence of a significant CO_2 stripping due to the overall CO_2 limitation in the process (Figure 2b). The slightly higher aqueous CO_2 concentration in the anoxic tank during SII and SIII mediated by biogas scrubbing supported a desorption of CO_2 from the anoxic tank, resulting in IC REs of 29±12% and 30±6%, respectively.

< Figure 2>

TN-REs in the anoxic tank increased from 18±8% in SI to 50±6% and 50±7% in SII and SIII, respectively (Figure 2c). This increase in TN removal was likely induced by the enhanced nitrification in the photobioreactor mediated by biogas supplementation, which ultimately promoted $N\text{-}NO_2^-$ and $N\text{-}NO_3^-$ reduction in the anoxic tank using the organic matter present in the influent wastewater. In fact, $N\text{-}NO_2^-$ and $N\text{-}NO_3^-$ represented the main e^- acceptors in SII and SIII, with a contribution to TOC oxidation of 56% and 60%, respectively. The steady state removals of $N\text{-}NH_4^+$ remained low at 6±14%, 9±11% and 2±7% during SI, SII and SIII, respectively. NH_4^+ removal in the anoxic tank was due to biomass assimilation mediated by heterotrophic TOC removal, which remained constant regardless of the operational stage (Figure 2d). $N\text{-}NO_2^-$ concentrations in the anoxic tank under steady state operation were negligible (0.01±0.01 mg/L, 0.03±0.05 and 0.41±0.68 in SI, SII and SIII, respectively). Likewise, $N\text{-}NO_3^-$ concentrations recorded in the anoxic tank in SI, SII and SIII were 0.04±0.03mg/L, 0.14±0.15mg/L and 0.73±1.25mg/L, respectively (Figure 3). These findings confirmed that both NO_2^- and NO_3^- derived from the photobioreactor and settler via the internal and external recirculations were efficiently reduced.

< Figure 3>

Negative overall $P\text{-}PO_4^3$-REs of -17±31% were recorded in the anoxic tank under steady state operation, with $P\text{-}PO_4^{3-}$ removals of -14±36%, -18±29% and -20±25% during SI, SII and SIII, respectively (Figure 2e). These negative $P\text{-}PO_4^3$-REs indicated that P was released by the algal-bacterial consortium in the absence of an e^- acceptor (nitrite, nitrate and dissolved oxygen) during SI, SII and SIII, respectively. In this context, recent studies have reported the ability of microalgae to accumulate non-structural $P\text{-}PO_4^{3-}$ under aerobic conditions, which is then released in the absence of e^- acceptor

(similarly to phosphate accumulating organisms, PAOs) [30][31]. In addition, the DGGE-sequencing analysis revealed the presence of heterotrophic bacteria with the ability to accumulate energy in the form of polyphosphate under excess of e^- acceptor and use this energy under anoxic conditions with the subsequent release of PO_4^{3-} to the culture medium. Hence, PAOs from the genus *Acinetobacter* (SI, SII and SIII), *Luteolibacter* (SI, SII and SIII), *Thauera* (SII and SIII), *Pseudomonas* (SIII), and *Aeromonas* (SI and SIII) were identified (supplementary materials Table S1) [29][32].

3.2.Carbon and nutrient removal in the photobioreactor

The TOC-REs under steady state operation in the photobioreactor averaged 12±5% regardless of the operational stage as a result of the efficient removal of organic matter in the anoxic tank (Figure 2a). The consistent concentrations of TOC 19±3 mg/L in the effluent over the entire experiment allowed us to estimate the fraction of non-biodegradable organic matter in the influent RWW to 11%. IC-REs in the photobioreactor under steady state condition accounted for 86±27% as a result of the intensive photosynthetic activity during the illuminated period along the three operational stages in the photobioreactor (Figure 2b). IC was almost completely depleted during the SI (supplementary material Figure S2b). The occurrence of IC limitation during SI supported the addition of biogas in order to supply an additional CO_2 source. Even under CO_2 supplementation, high IC-REs of 63±10% and 62±7% were recorded during SII and SIII, respectively. The enhanced IC availability mediated by biogas upgrading entailed an increase in the concentration of algal-bacterial biomass.

Low TN-REs of 20±7% were recorded under SI steady state, which increased up to 30±7% and 32±9% in SII and SIII, respectively, as a result of the higher biomass

production induced by biogas supplementation (Figure 2c). Likewise, while IC limitation mediated low N-NH_4^+-REs (33±20%) during SI, the increase in nitrification activity supported by CO_2 supplementation increased N-NH_4^+-REs up to 89±11% and 96±7% in SII and SIII, respectively (Figure 2d and supplementary material Figure S2d). N-NO_2^- was the dominant form of oxidized nitrogen (N-NO_2^- = 5.6±4.0 mg/L *vs* N-NO_3^- =0.9±0.9 mg/L) during SI (Table 1 and Figure 3). CO_2 supplementation via biogas upgrading promoted nitrification, which resulted in a decrease in N-NO_2^- concentration to 3.1±3.8 mg/L concomitant with an increase in N-NO_3^- concentration up to 8.9±5.5 mg/L in SII [29]. Likewise, an almost complete nitrification was achieved during steady SIII, with N-NO_3^- and N-NO_2^- of 13.0±3.2 mg/L and 1.1±1.8 mg/L of N-NO_2^-, respectively.

The overall steady state P-PO_4^{3-}-REs in the photobioreactor accounted for 80±39%, with values of 73±49%, 85±28% and 81±29% in SI, SII and SIII, respectively (Figure 2e). P assimilation into algal-bacterial biomass was the most likely removal mechanism in the photobioreactor based on the range of pH values recorded during illuminated periods (6.8-9.4) and (6.4-8.1) during the dark periods in SII and SIII.

3.3. Biomass concentration and sludge volumetric index

TSS concentration in the anoxic tank increased from 1519±252 mg TSS/L in SI to 3113±361 mg TSS/L and 2480±309 mg TSS/L during SII and SIII, respectively (Table 1 and Figure 4a). Likewise, biomass concentration in the aerobic tank under steady state operation accounted for 1216±260 mg TSS/L, 2854±324mg TSS/L and 2047±186 mg TSS/L in SI, SII and SIII, respectively.

The fact that TOC removal remained similar along the three operational stages clearly showed that the increase in biomass concentration recorded during SII and SIII was mediated by the enhanced growth of autotrophic microbial communities (microalgae, cyanobacteria and nitrifying bacteria). Finally, effluent TSS concentrations during steady state gradually decreased from 163±83 mg TSS/L in SI, to 81±45 mg TSS/L in SII and 26±12 mg TSS/L in SIII (Figure 4a). The value obtained under steady state in SIII enabled compliance with the European Directive 97/271/CEE [33].

< Figure 4>

The sludge volumetric index recorded at the end of SI in the anoxic tank and photobioreactor accounted for 95 mL TSS/g and 161 mL TSS/g, respectively (Table 1 and Figure 4b). Surprisingly, the enhanced sedimentation observed during SII, based on the decrease in the effluent TSS concentrations, was not correlated with the SVI in the anoxic tank (128 mL TSS/g) or in the photobioreactor (169 mL TSS/g). These high SVI were likely due to the presence of the filamentous bacteria *Caldilineae* in SI and SII and *Clostridium* in SI, SII and SIII. However, the decrease in SVI recorded during SIII in both the anoxic tank and photobioreactor (80 mL TSS/g and 97 mL TSS/g, respectively) was correlated with low effluent TSS concentrations (Figures 4a and 4b). Overall, SVI of 50 - 100 mL/g in activated sludge plants are considered an indication of a good biomass settling [29]. Low SVI were also reported by Alcántara et al. (2015) in a photobioreactor designed with a continuous biomass recycling. Park et al. (2011) also reported an increase in microalgae settleability by 20% when implementing biomass recycling strategies in HRAPs, which confirmed the key of role of this operational strategy to enhance biomass settling [14][34]. The settling rates of biomass present in the anoxic tank accounted for 1.86 m/h, 1.20 m/h and 1.44 m/h in SI, SII and SIII,

respectively. Settling rates of 1.56m/h, 1.02 m/h and 1.47 m/h were recorded for the biomass present in the photobioreactor in SI, SII and SIII, respectively. An analysis of variance confirmed that the biomass present in the anoxic tank exhibited higher settling rates than the biomass in the photobioreactor in SI and SII. The results here obtained were comparable with those reported by de Godos et al. (2014) and higher than the rates obtained by Alcántara et al. (2015) using a similar AA-ABPh [13][14]. Similarly, 80% of algal biomass present in a HRAP treating domestic WW at 4 days of HRTs exhibited rates higher than 0.4 m/h (Gutierrez et al. 2016) [35].

3.4 Dynamics of microalgae and bacteria population

Morphological characterization of microalgae population structure revealed a gradual dominance of the genus *Scenedesmus*, which accounted for 46 % of total microalgae population in the absence of biogas supply, and for 94-100% when CO_2 was supplemented to the wastewater treatment process (Figure 5). *Desmodesmus spinosus*, *Pseudanabaena sp.*, *Leptolyngbya benthonica* and *Acutodesmus obliquus* represented 38%, 30%, 23% and 8% of the total microalgae population in SI, respectively. In SII, *Leptolyngbya benthonica* and *Pseudanabaena sp* were gradually replaced by *Desmodesmus spinosus* and *Acutodesmus obliquus,* which accounted for 50% and 44% of the total population, respectively. Finally, microalgae population in SIII became dominated by *Desmodesmus spinosus* (76%) and *Scenedesmus tenuispina* (24%). *Scenedesmus* species is commonly found in HRAPs treating domestic WW [36] because of their tolerance to high nitrogen and organic matter concentrations [37][38]. This study suggests that biomass sedimentation and recycling can contribute to the enrichment of monoalgal microalgae species with good settling properties. Previous studies in pilot HRAPs conducted with biomass recycling promoted the dominance of

unialgal cultures [34]. In this context, biomass settling and recycling also resulted in the dominance of *Micractinium sp* and *Scenedesmus sp* in HRAPs treating RWW with an external CO_2 supplementation [27].

< Figure 5>

DGGE analysis of the bacterial community in the photobioreactor revealed the occurrence of 10 phyla and 33 bands (Figure 6 and supplementary material Table S1). *Proteobacteria*, which are ubiquitous in the environment, was the dominant phylum with 17 bands of the 33 sequenced. The phylum *Proteobacteria* was the most dominant with 9, 9, 6 and 12 bands detected in the inoculum, SI, SII and SIII, respectively (Figure 6 and supplementary material Table S1)[39]. The analysis also identified the phyla *Acidobacteria*, *Verrucomicrobia*, *Firmicutes* and *Actinobacteria* with two bands each, the phyla *Chloroflexi*, *Cyanobacteria/Chloroplast*, *Gemmatimonadetes*, *Ignavibacteriae*, *Candidatus Saccharibacteria* with one band and 3 unclassified bacteria. Bacteria from the phyla *Proteobacteria, Acidobacteria, Actinobacteria* and *Firmicutes* were likely responsible for the degradation of organic matter in both the anoxic and photobioreactor tanks. Bacteria from the above mentioned phyla are typically found in activated sludge WWTP, autotrophic nitrifying and denitrifying bioreactors and HRAPs. More specifically, denitrifying bacteria such as *Pseudomonas* (SIII), *Litorilinea* (SI and SII), *Gp4* (SII) and *Thauera* (SII and SIII) were identified (Figure 6 and supplementary material Table S1).

Likewise, nitrifying bacteria belonging to the family *Xhantomonadaceae* (SI, SII and SIII) and genus *Aeromonas* (SI and SIII), *Aquamicrobium* (SI, SII and SIII), *Luteliobacter* (SI, SII and SIII), *Thauera* (SII and SIII) *and Gp4* (SII) were detected as a result on the increased availability of CO_2.

< Figure 6>

The Shannon-Weiner diversity index (H) for the inoculum (S0) and the population established in the different operational stages showed a high bacterial diversity. The Shannon-Weiner diversity index typically ranges from 1.5 to 3.5, higher H values corresponding to a higher species richness and evenness [16][20]. In this study, H indexes of 3.4, 3.5, 3.2 and 3.2 were estimated in the inoculum and in the microbial populations established during SI, SII and SIII, respectively (Figure 6). HRAPs treating WW typically exhibit H indexes ranging from 3.0 to 3.5, which confirms the high robustness and functionality of the microbiology present in algal-bacterial processes. Both the H index and the DGGE band profile clearly showed that biogas supplementation in SII and SIII stabilized the bacterial community. The analysis of the similarity indexes showed a lower similarity between the inoculum (S0) and the population in SI (25.4%), than the similarity between the populations in SI and II (63.2 %) in SII and SIII (41.30%), which indicated a functional specialization to the host environment during the experiment [40].

3.5 Biogas upgrading

CO_2 supplementation via biogas upgrading was crucial to ensure an efficient nitrification in the photobioreactor and further denitrification in the anoxic tank. CO_2 removal from biogas in the absorption column averaged 92±2% and 93±2 % during steady state II and III, respectively (Figures 7a). H_2S was completely removed from biogas regardless of the operational stage as a result of its higher solubility compared to CO_2 (Figure 7b). The results obtained here were in agreement with the REs of 80% for CO_2 and 100% for H_2S reported by other authors in HRAPs devoted to biogas

upgrading using a similar L/G ratio of ≈ 10 (v/v) [12][41]. While CO_2 supplied was assimilated by nitrifying bacteria and microalgae, H_2S was rapidly oxidized to SO_4^{2-} using the O_2 photosynthetically produced in the photobioreactor. In this context, the removal efficiencies of SO_4^{2-} in the anoxic tank accounted for 92±54% and 16±50% during steady state II and III, respectively (Figure 7c). On the other hand, SO_4^{2-}-REs of -140±58% and -83±60% were recorded in the photobioreactor during steady state II and III, respectively, as a result of SO_4^{2-} production from H_2S oxidation (Figure 7b and 7c). The DGGE sequencing analysis revealed the presence of the H_2S degrading strain *Pseudomonas frederiksbergensis* NR_117177, which supported the biological oxidation of H_2S in the system (Supplementary material Table S1) [42][43].

< Figure 7>

4. Conclusion

The novel anoxic-aerobic algal-bacterial photobioreactor coupled with a biogas upgrading unit here evaluated exhibited consistent C, N and P removal efficiencies. CO_2 supplementation from biogas was required to overcome the overall IC limitation recorded in SI, and supported both an efficient nitrification-denitrification process and an enhanced N and P removal by assimilation during SII and SIII. This innovative process configuration also supported an efficient biogas upgrading, with CO_2 and H_2S removal efficiencies of 85 and 100 %, respectively. Continuous biomass settling and recycling promoted the enrichment of an unialgal culture by the end of the experiment. Finally, DGGE-sequencing analysis confirmed that biogas supplementation promoted the development of nitrifying, denitrifying and H_2S degrading bacteria during SII and SIII.

References

[1] FAO, The State of the World's land and water resources for Food and Agriculture. Managing systems at risk, 2011. doi:978-1-84971-326-9.

[2] U.S. Enviromental Protection Agency, CLIMATE CHANGE INDICATOR IN THE UNITED STATES 2016, Fourth edi, 2016. www.epa.gov/climate-indicators.

[3] J. Ruiz, P.D. Álvarez-Díaz, Z. Arbib, C. Garrido-Pérez, J. Barragán, J.A. Perales, Performance of a flat panel reactor in the continuous culture of microalgae in urban wastewater: Prediction from a batch experiment, Bioresour. Technol. 127 (2013) 456–463. doi:10.1016/j.biortech.2012.09.103.

[4] Z. Arbib, J. Ruiz, P. Álvarez-Díaz, C. Garrido-Pérez, J.A. Perales, Capability of different microalgae species for phytoremediation processes: Wastewater tertiary treatment, CO2 bio-fixation and low cost biofuels production, Water Res. 49 (2014) 465–474. doi:10.1016/j.watres.2013.10.036.

[5] A. Ruiz-Martinez, N. Martin Garcia, I. Romero, A. Seco, J. Ferrer, Microalgae cultivation in wastewater: nutrient removal from anaerobic membrane bioreactor effluent., Bioresour. Technol. 126 (2012) 247–253. doi:10.1016/j.biortech.2012.09.022.

[6] R. Muñoz, B. Guieysse, Algal-bacterial processes for the treatment of hazardous contaminants: A review., Water Res. 40 (2006) 2799–2815. doi:10.1016/j.watres.2006.06.011.

[7] M. Wang, H. Yang, S.J. Ergas, P. van der Steen, A novel shortcut nitrogen removal process using an algal-bacterial consortium in a photo-sequencing batch reactor (PSBR), Water Res. 87 (2015) 38–48. doi:10.1016/j.watres.2015.09.016.

[8] L. Christenson, R. Sims, Production and harvesting of microalgae for wastewater treatment, biofuels, and bioproducts., Biotechnol. Adv. 29 (2011) 686–702. doi:10.1016/j.biotechadv.2011.05.015.

[9] J.B.K. Park, R.J. Craggs, A.N. Shilton, Investigating why recycling gravity harvested algae increases harvestability and productivity in high rate algal ponds., Water Res. 47 (2013) 4904–4917. doi:10.1016/j.watres.2013.05.027.

[10] I. de Godos, V.A. Vargas, S. Blanco, M.C. García González, R. Soto, P.A. García-Encina, et al., A comparative evaluation of microalgae for the degradation of piggery wastewater under photosynthetic oxygenation, Bioresour. Technol. 101 (2010) 5150–5158. doi:10.1016/j.biortech.2010.02.010.

[11] C. Alcántara, P.A. García-Encina, R. Muñoz, Evaluation of mass and energy balances in the integrated microalgae growth-anaerobic digestion process, Chem. Eng. J. 221 (2013) 238–246. doi:10.1016/j.cej.2013.01.100.

[12] M.L. Serejo, E. Posadas, M.A. Boncz, S. Blanco, P. García-Encina, R. Muñoz, Influence of Biogas Flow Rate on Biomass Composition During the Optimization of Biogas Upgrading in Microalgal-Bacterial Processes, Environ. Sci. Technol. (2015) 150212112813001. doi:10.1021/es5056116.

[13] I. de Godos, V.A. Vargas, H.O. Guzmán, R. Soto, B. García, P.A. García, et al., Assessing carbon and nitrogen removal in a novel anoxic-aerobic cyanobacterial-bacterial photobioreactor configuration with enhanced biomass sedimentation., Water Res. 61 (2014) 77–85. doi:10.1016/j.watres.2014.04.050.

[14] C. Alcántara, J.M. Domínguez, D. García, S. Blanco, R. Pérez, P.A. García-Encina, et al., Evaluation of wastewater treatment in a novel anoxic-aerobic algal-bacterial photobioreactor with biomass recycling through carbon and nitrogen mass balances, Bioresour. Technol. 191 (2015) 173–186.

doi:10.1016/j.biortech.2015.04.125.

[15] APHA, Standards Methods for the Examination of Water and Wastewater, 21 st, American Public Health Association, American Water Works Association, Water Enviroment Federation, Washington,D.C, 2005. https://www.standardmethods.org/.

[16] J.C. López, G. Quijano, R. Pérez, R. Muñoz, Assessing the influence of CH4 concentration during culture enrichment on the biodegradation kinetics and population structure., J. Environ. Manage. 146 (2014) 116–123. doi:10.1016/j.jenvman.2014.06.026.

[17] A. Sournia, Phytoplankton manual, UNESCO, Paris, 1978. http://unesdoc.unesco.org/images/0003/000307/030788eo.pdf.

[18] U. Nübel, B. Engelen, A. Felske, J. Snaidr, A. Wieshuber, R.I. Amann, et al., Sequence heterogeneities of genes encoding 16S rRNA in Paenibacillus polymyxy detected by temperature gradient gel electrophoresis., J. Bacteriol. 178 (1996) 5636–5643.

[19] K. Roest, H.G.H.J. Heilig, H. Smidt, W.M. de Vos, A.J.M. Stams, A.D.L. Akkermans, Community analysis of a full-scale anaerobic bioreactor treating paper mill wastewater., Syst. Appl. Microbiol. 28 (2005) 175–185. doi:10.1016/j.syapm.2004.10.006.

[20] G.M. MacDonald, Space , Time , and Life, John Wiley & Sons, Inc, New York, USA, 2003.

[21] B.G. Häne, K. Jäger, H.G. Drexler, The Pearson product-moment correlation coefficient is better suited for identification of DNA fingerprint profiles than band matching algorithms, Electrophoresis. 14 (1993) 967–972. doi:10.1002/elps.11501401154.

[22] H.-F. Wang, W.-Y. Zhu, W. Yao, J.-X. Liu, DGGE and 16S rDNA sequencing analysis of bacterial communities in colon content and feces of pigs fed whole crop rice., Anaerobe. 13 (2007) 127–133. doi:10.1016/j.anaerobe.2007.03.001.

[23] S. McGinnis, T.L. Madden, BLAST: At the core of a powerful and diverse set of sequence analysis tools, Nucleic Acids Res. 32 (2004) 20–25. doi:10.1093/nar/gkh435.

[24] E. Posadas, M.D.M. Morales, C. Gomez, F.G. Acién, R. Muñoz, Influence of pH and CO2 source on the performance of microalgae-based secondary domestic wastewater treatment in outdoors pilot raceways, Chem. Eng. J. 265 (2015) 239–248. doi:10.1016/j.cej.2014.12.059.

[25] J. García, R. Mujeriego, M. Hernandez-Mariné, High rate algal pond operating strategies for urban wastewater nitrogen removal, Appl. Phycol. 12 (2000) 331–339. doi:10.1023/a:1008146421368.

[26] J. Mata Álvarez, F. Fdez-Polanco, Ecoeficiencia en la EDAR del Siglo XXI, Santiago de Compostela, España, 2010.

[27] S. Heubeck, R.J. Craggs, A. Shilton, Influence of CO2 scrubbing from biogas on the treatment performance of a high rate algal pond, Water Sci. Technol. 55 (2007) 193–200. doi:10.2166/wst.2007.358.

[28] G. Tchobanoglous, H.D. Stensel, R. Tsuchihashi, F. Burton, Wastewater Engineering Treatment and Resource Recovery, Fifth edit, McGraw-Hill Education, 2014. www.mhhe.com.

[29] B.E. Rittmann, P.L. Mccarty, Environmental Biotechnology:Principles and Applications, 1 st, Tata McGraw-Hill, New Delhi, 2012.

[30] C. Alcántara, C. Fernández, P.A. García-Encina, R. Muñoz, Mixotrophic metabolism of Chlorella sorokiniana and algal-bacterial consortia under extended

dark-light periods and nutrient starvation, Appl. Microbiol. Biotechnol. 99 (2015) 2393–2404. doi:10.1007/s00253-014-6125-5.

[31] L.E. De-Bashan, Y. Bashan, Recent advances in removing phosphorus from wastewater and its future use as fertilizer (1997-2003), Water Res. 38 (2004) 4222–4246. doi:10.1016/j.watres.2004.07.014.

[32] J. Yoon, Y. Matsuo, K. Adachi, M. Nozawa, S. Matsuda, H. Kasai, et al., Description of Persicirhabdus sediminis gen. nov., sp. nov., Roseibacillus ishigakijimensis gen. nov., sp. nov., Roseibacillus ponti sp. nov., Roseibacillus persicicus sp. nov., Luteolibacter pohnpeiensis gen. nov., sp. nov. and Luteolibacter algae sp. no, Int. J. Syst. Evol. Microbiol. 58 (2008) 998–1007. doi:10.1099/ijs.0.65520-0.

[33] CEC, Consejo de las Comunidaes Europeas. Directiva del Consejo sobre el tratamiento de las aguas residuales urbanas (91/271/CEE), (1991) 40–52.

[34] J.B.K. Park, R.J. Craggs, A.N. Shilton, Recycling algae to improve species control and harvest efficiency from a high rate algal pond., Water Res. 45 (2011) 6637–6649. doi:10.1016/j.watres.2011.09.042.

[35] R. Gutiérrez, I. Ferrer, E. Uggetti, C. Arnabat, H. Salvadó, J. García, Settling velocity distribution of microalgal biomass from urban wastewater treatment high rate algal ponds, Algal Res. 16 (2016) 409–417. doi:10.1016/j.algal.2016.03.037.

[36] I. de Godos, V.A. Vargas, H.O. Guzmán, R. Soto, B. García, P.A. García, et al., Assessing carbon and nitrogen removal in a novel anoxic-aerobic cyanobacterial-bacterial photobioreactor configuration with enhanced biomass sedimentation, Water Res. 61 (2014) 77–85. doi:10.1016/j.watres.2014.04.050.

[37] S. Canovas, B. Picot, C. Casellas, H. Zulkifi, A. Dubois, J. Bontoux, Seasonal development of phytoplankton and zooplankton in a high-rate algal pond, Water

Sci. Technol. 33 (1996) 199–206. doi:10.1016/0273-1223(96)00355-1.

[38] C.. Palmer, A composite rating of algae tolerating organic pollution, J. Phicology. 5 (1969) 78–82.

[39] N.-R. Shin, T.W. Whon, J.-W. Bae, Proteobacteria: microbial signature of dysbiosis in gut microbiota., Trends Biotechnol. 33 (2015) 496–503. doi:10.1016/j.tibtech.2015.06.011.

[40] O.H. Diserud, F. Ødegaard, A multiple-site similarity measure, Biol. Lett. 3 (2007) 20–22. http://www.ncbi.nlm.nih.gov/pmc/articles/PMC2373804/.

[41] M. Bahr, I. Díaz, A. Dominguez, A. González Sánchez, R. Muñoz, Microalgal-biotechnology as a platform for an integral biogas upgrading and nutrient removal from anaerobic effluents, Environ. Sci. Technol. 48 (2014) 573–581. doi:10.1021/es403596m.

[42] W. Adam, F. Heckel, C.R. Saha-Möller, M. Taupp, J.-M. Meyer, P. Schreier, Opposite enantioselectivities of two phenotypically and genotypically similar strains of Pseudomonas frederiksbergensis in bacterial whole-cell sulfoxidation, Appl. Environ. Microbiol. 71 (2005) 2199–2202. doi:10.1128/AEM.71.4.2199-2202.2005.

[43] S.M. Andersen, K. Johnsen, J. Sørensen, P. Nielsen, C.S. Jacobsen, Pseudomonas frederiksbergersis sp. nov., isolated from soil at a coal gasification site, Int. J. Syst. Evol. Microbiol. 50 (2000) 1957–1964.

Acknowledgments

This research was supported by the Spanish Ministry of Economy and Competitiveness and FEDER EU program (CTM2015-70442-R) the Regional Government of Castilla y León (Project VA024U14 and UIC 71) and INIA (RTA2013-00056-C03-02). The financial support of the program ERASMUS MUNDUS: EURICA and Universidad Nacional Autónoma de Nicaragua (UNAN-Managua) are also gratefully acknowledged.

Figure captions

Figure 1. Schematic diagram of the anoxic-aerobic algal-bacterial photobioreactor set-up coupled with an absorption column for CO_2 supplementation via biogas upgrading.

Figure 2. Removal efficiency of (a) TOC, (b) IC, (c) TN, (d) $N\text{-}NH_4^+$ and (e) $P\text{-}PO_4^{3-}$ in the anoxic tank (▨), aerobic photobioreactor (▩) and overall system (⬚) during the steady states achieved in the three operational stages evaluated. Vertical bars represent the standard deviation from replicate measurements during steady state operation.

Figure 3. Time course of nitrite (triangles) and nitrate (squares) in the anoxic tank (black) and photobioreactor (white) during the entire experiment. Vertical dashed lines separate the different operational stage evaluated.

Figure 4. Time course of (**a**) TSS concentration in the anoxic tank (♦) and aerobic tank (○) and effluent (×, secondary axis), and (**b**) **SVI** in the anoxic tank (■) and photobioreactor (□) during the steady states achieved in the three operational stages evaluated. Vertical dashed lines separate the different operational stages.

Figure 5. Microalgae population structure in the photobioreactor during the entire operational period: *Chlorella* ▧, *Pseudanabaena sp.*▨, *Leptolyngbya benthonica* ▤, *Nitzschia palea* ⁘, *Scenedesmus tenuispina* ▧, *Desmodesmus spinosus* ▦ and *Acutodesmus obliquus* ▥.

Figure 6. DGGE profile of the bacterial community present in the anoxic-aerobic algal-bacterial photobioreactor in the inoculum (S0), stage I (SI), stage II (SII) and stage III (SIII). Horizontal arrows and numbers indicate the most abundant bacterial communities. The name of the samples and the Shannon-Weiner diversity indexes are also depicted in the upper part of the gel.

Figure 7. Time course of the inlet (♦) and outlet (Δ) concentrations, and removal efficiency (▬) of CO_2 (a) and H_2S (b), in the absorption column during stage II and III, and (c) removal efficiency of SO_4^{2-} in the anoxic tank (▨), aerobic photobioreactor (▩) and overall system (⬚) during the steady states achieved in the three operational stages evaluated. Vertical bars represent the standard deviation from replicate measurements during steady state operation.

Table

Table 1. Operational conditions and physical/chemical characterization of the real wastewater and cultivation broth in the anoxic tanks and photobioreactor.

Stage		**Wastewater**	**SI**		**SII**		**SIII**	
Parameter / Reactor			**Anoxic**	**Aerobic**	**Anoxic**	**Aerobic**	**Anoxic**	**Aerobic**
Operational period (days)		n.a	78		74		56	
HRT (days)		n.a	0.5	1.5	0.5	1.5	0,5	1.5
SRT (days)		n.a	12.5 ± 3.5		11 ± 0.9		10.5 ± 0.5	
Light (µmol/m^2.s)		n.a	n.a	367±57	n.a	412±15	n.a	395±21
RWW feeding rate (L/d)		n.a	1.8		1.8		1.8	
Internal recycling rate (L/d)		n.a	2.8		2.8		3.6	
External recycling rate (L/d)		n.a	0.5		0.5		0.5	
pH (units)	***Light***	n.a	7.4±0.3	8.6±0.6	6.9±0.1	8.0±0.7	6.8±0.2	8.9±0.9
	Dark	n.a		7.1±0.3		7±0.2		7.0±0.4
Dissolved oxygen (mg/L)	***Light***	n.a	0	23.3±4.1	0	22.0±2.0	0	23.0±1.8
	Dark	n.a		6.0±0.6		3.1±1.2		3.9±0.7
TOC (mg/L)		176±26	26±5	20±4	30±4	19±1	23±2	18±2
IC (mg/L)		152±34	48±5	2±1	56±9	15±5	47±4	13±4
TN (mg/L)		106±9	74±10	66±8	32±4	21±3	28±2	18±4
N-NH_4^+ (mg/L)		93±9	64±4	54±8	32±5	3±1	33±2	3±1
N-NO_2^- (mg/L)		n.a	0.01±0.01	5.6±4.0	0.03±0.05	3.1±3.8	0.41±0.68	1.1±1.8
N-NO_3^- (mg/L)		n.a	0.04±0.03	0.9±0.9	0.14±0.15	8.9±5.5	0.73±1.25	13.0±3.2
P-PO_4^{3-} (mg/L)		33±8	26±5	16±7	18±3	9±2	18±1	11±2
SO_4^{2-}		39±12	29±7	32±6	51±15	76±11	47±7	55±4
TSS (mg/L)		n.a	1519±252	1216±260	3113±361	2854±324	2480±309	2047±186
SVI (mL/g)		n.a	95	161	128	169	80	97
Air flow (mL/min)		n.a	0	6	0	4	0	2
Biogas (L/day)		n.a	n.a			2.6		2.6
n.a : Not applicable								

Figure

Figure 1.

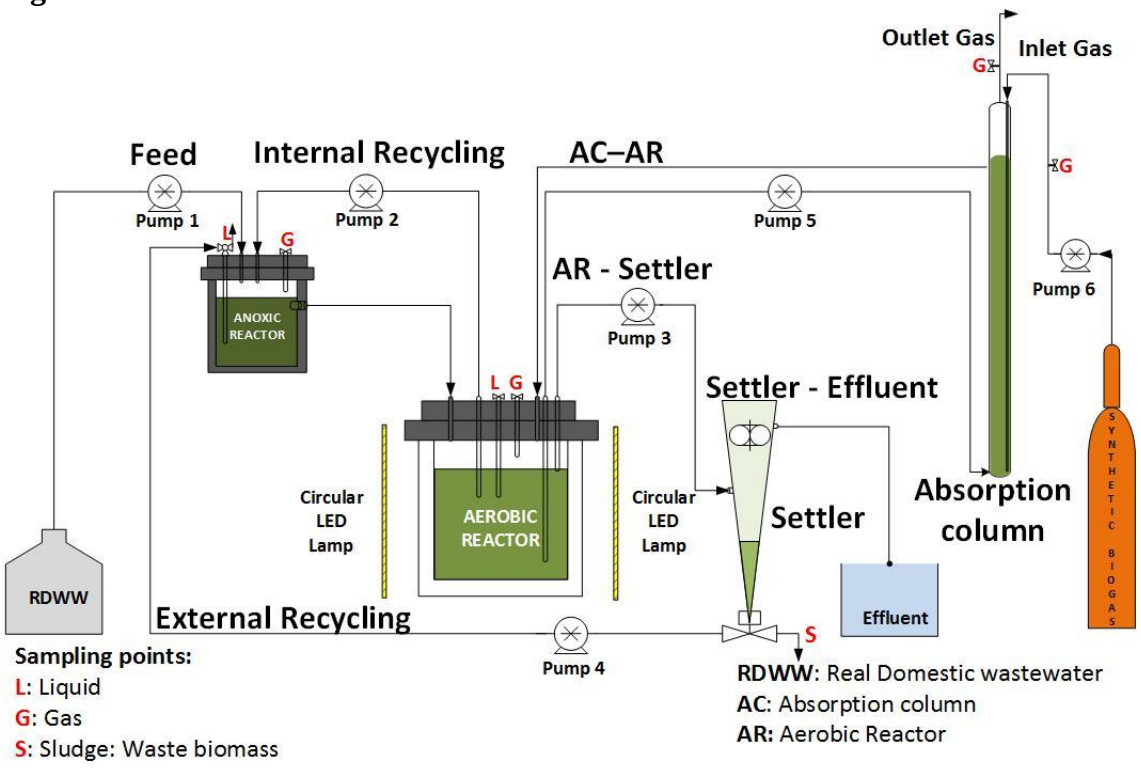

Figure 1. Schematic diagram of the anoxic-aerobic algal-bacterial photobioreactor set-up coupled with an absorption column for CO_2 supplementation via biogas upgrading.

Figure 2.

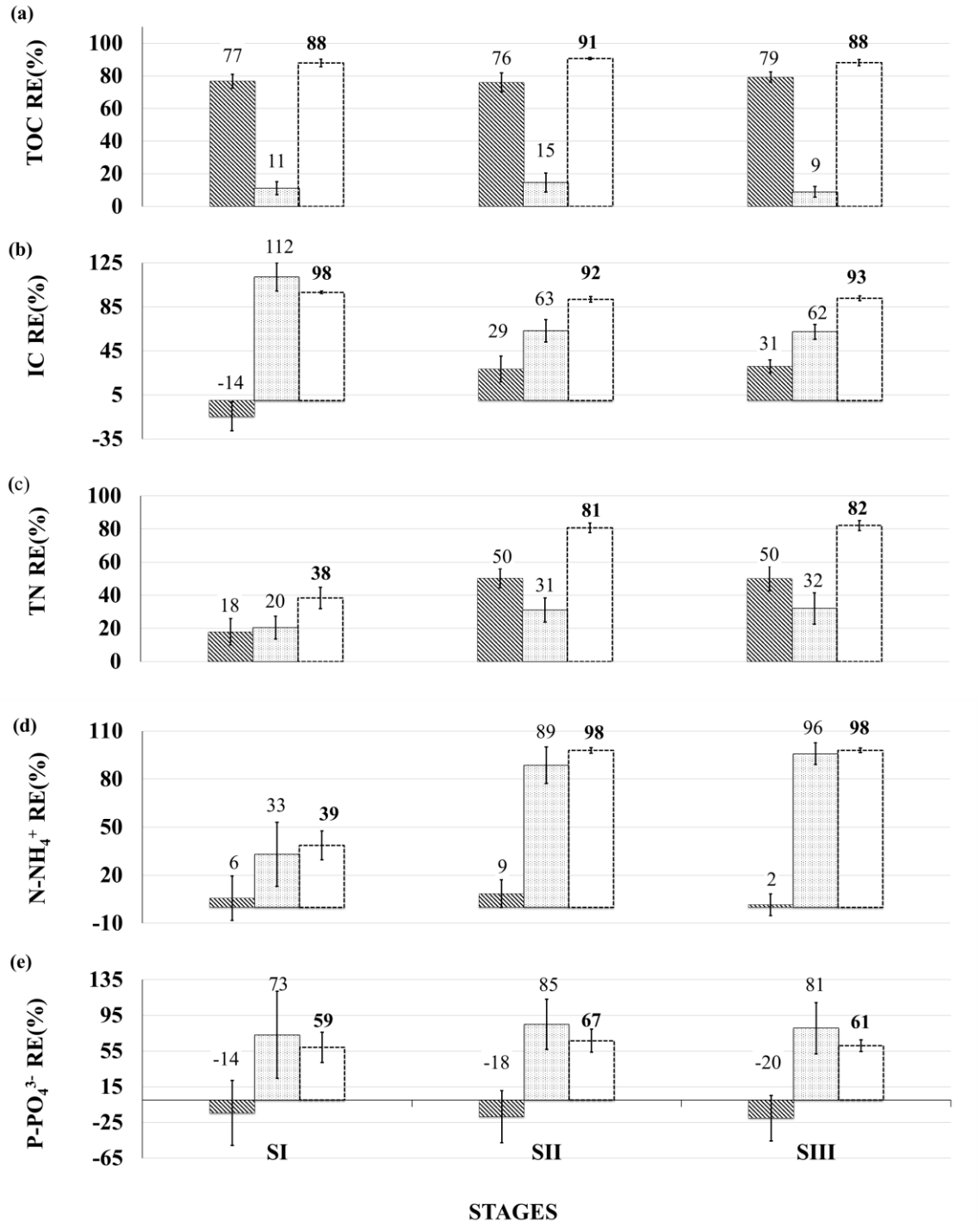

Figure 2. Removal efficiency of (a) TOC, (b) IC, (c) TN, (d) $N\text{-}NH_4^+$ and (e) $P\text{-}PO_4^{3-}$ in the anoxic tank (▨), aerobic photobioreactor (▩) and overall system (⬚) during the steady states achieved in the three operational stages evaluated. Vertical bars represent the standard deviation from replicate measurements during steady state operation.

Figure 3.

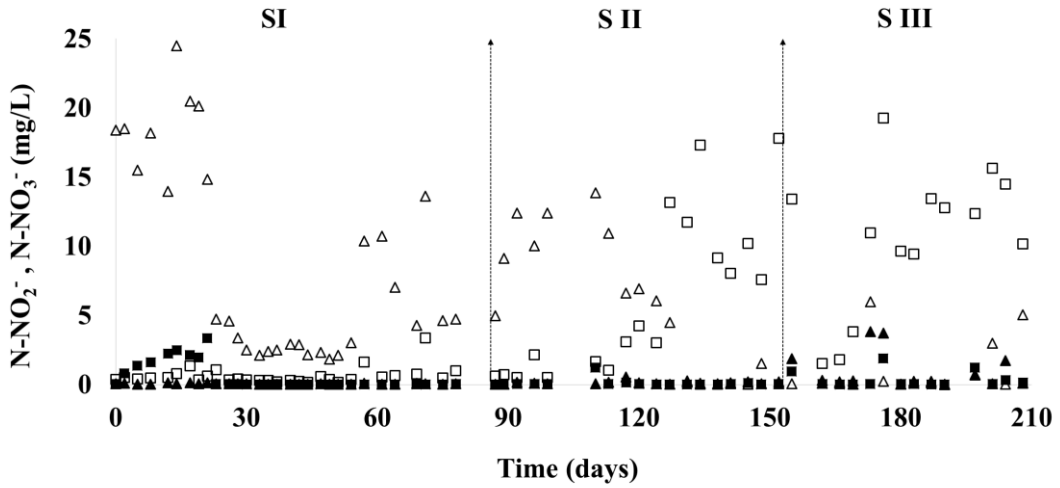

Figure 3. Time course of nitrite (triangles) and nitrate (squares) concentrations in the anoxic tank (black) and photobioreactor (white) during the entire experiment. Vertical dashed lines separate the different operational stages evaluated.

Figure 4.

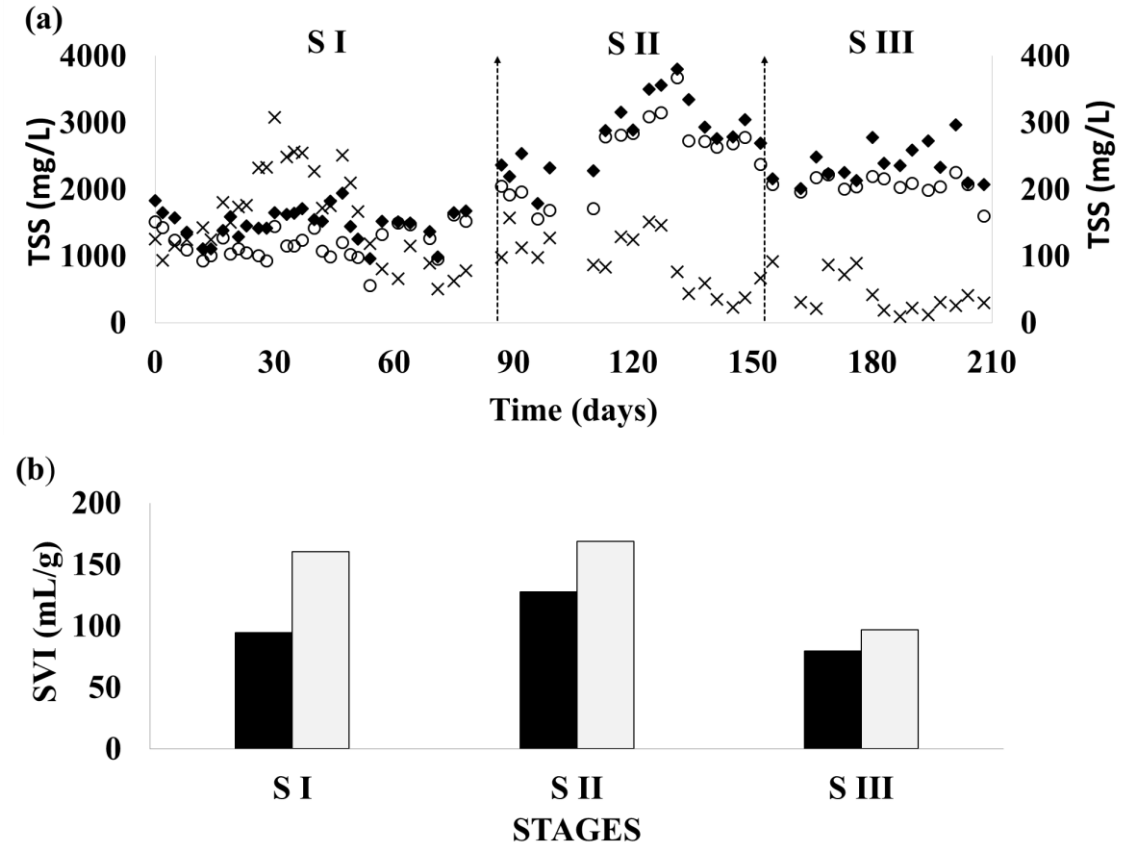

Figure 4. Time course of (**a**) TSS concentration in the anoxic tank (♦) and aerobic tank (○) and effluent (×, secondary axis), and (**b**) **SVI** in the anoxic tank (■) and photobioreactor (□) during the steady states achieved in the three operational stages evaluated. Vertical dashed lines separate the different operational stages.

Figure 5.

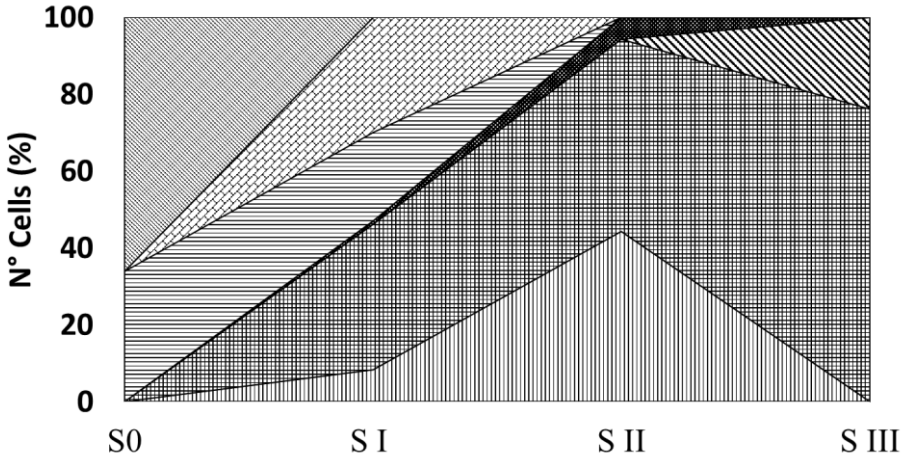

Figure 5. Microalgae population structure in the photobioreactor during the entire operational period: *Chlorella*, *Pseudanabaena sp.*, *Leptolyngbya benthonica*, *Nitzschia palea*, *Scenedesmus tenuispina*, *Desmodesmus spinosus* and *Acutodesmus obliquus*.

Figure 6.

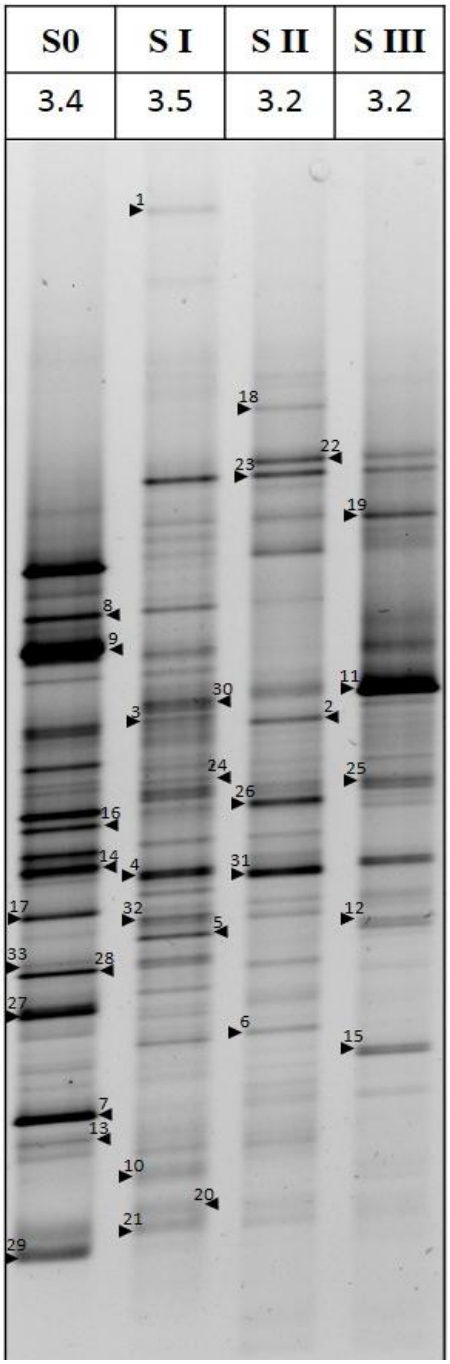

Figure 6. DGGE profile of the bacterial community present in the anoxic-aerobic algal-bacterial photobioreactor in the inoculum (S0), stage I (SI), stage II (SII) and stage III (SIII). Horizontal arrows and numbers indicate the most abundant bacterial communities. The name of the samples and the Shannon-Weiner diversity indexes are also depicted in the upper part of the gel.

Figure 7.

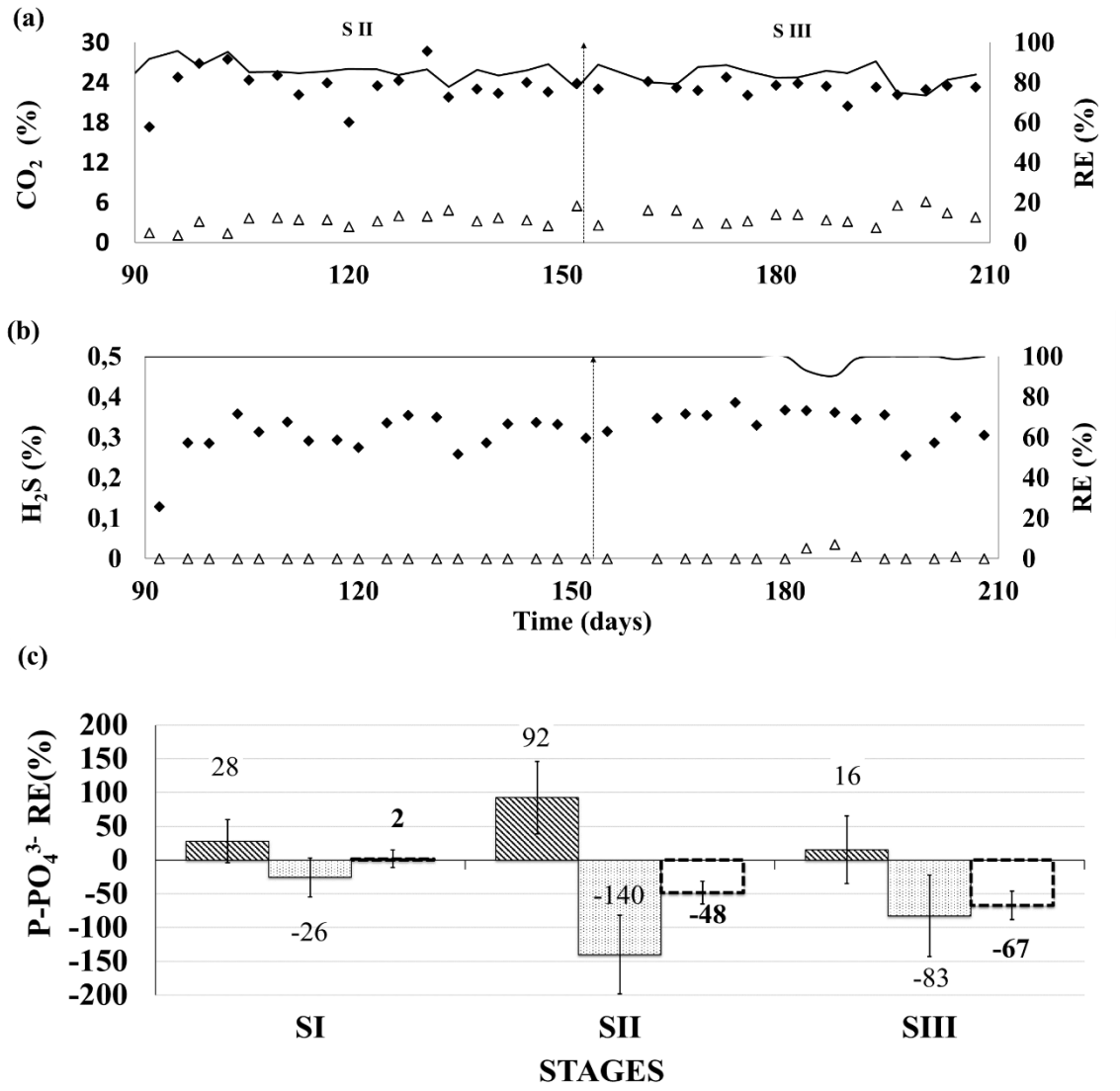

Figure 7. Time course of the inlet (♦) and outlet (Δ) concentrations, and removal efficiency (▬) of CO_2 (a) and H_2S (b), in the absorption column during stage II and III, and (c) removal efficiency of SO_4^{2-} in the anoxic tank (▨), aerobic photobioreactor (▩) and overall system (⬚) during the steady states achieved in the three operational stages evaluated. Vertical bars represent the standard deviation from replicate measurements during steady state operation.

Supplementary Material

Click here to download Supplementary Material: Supplementarymaterials_Garcia.docx